Microsystem Technologies (2021) 27:2803–2813
https://doi.org/10.1007/s00542-020-05070-7

TECHNICAL PAPER

Analysis and design of a novel high capacitance ratio and low actuation voltage RF MEMS switch

Kun Deng[1] · Fuxing Yang[1] · Zhongliang Deng[2] · Xuanming Wang[2] · Ke Han[2]

Received: 22 August 2020 / Accepted: 13 October 2020 / Published online: 24 October 2020
© Springer-Verlag GmbH Germany, part of Springer Nature 2020

Abstract

Analysis and design of a novel high on/off capacitance ratio and low actuation voltage radio frequency microelectromechanical systems (RF MEMS) switch. Circuit topology and electrode topology of RF MEMS switches are analyzed. In order to decrease actuation voltage, the switch, using coplanar waveguide transmission line for signal transmission, are designed with special elastic supported structures and actuation electrode are located on both sides of signal line. Metal–insulator–metal (MIM) fixed capacitors are used to change the up/down-state capacitance without adding more loss to the switches. Through the finite element method to determine the spring constant and the necessary applied voltage, the simulation voltage is 4.5 V. The RF performance are obtained by simulating results in the HFSS tool. The switch exhibits the insertion loss of -0.2 dB, and isolation of -20 dB within the range of 10–30 GHz, and the isolation extreme value reaches -41 dB at resonant frequency, the return loss is less than -12 dB at the resonant frequency. From the fitted results, the on/off capacitance ratio is 162 for the MEMS switch. Compared with traditional MEMS capacitive switches, the proposed MEMS switch exhibit high on/off capacitance ratios and low actuation voltage.

1 Introduction

In such an era of scaling down semiconductor devices in micro or nanometer range, RF MEMS switch with the advantages of low or near-zero power consumption, high isolation, low insertion loss, and high linearity has obtained a rapid development (Metta et al. 2018). Compared to PIN diode or FET switches, RF MEMS switch is more suitable for high frequency and miniaturized communication system. The traditional capacitive RF MEMS switch is electrostatically actuated, and it contains a coplanar waveguide to transmit signals, a big suspended membrane as actuator and an electrode to provide bias voltage. When a voltage bias is applied, the switch use mechanical movements to short or open a transmission.

Capacitance ratio and actuation voltage are two important indexes to measure the switch performance. The former reflects the RF performance of the switch, while the latter reflects the mechanical characteristic of the switch. However, the two are often mutually limited in design. A simple and effective approach to obtain high on/off capacitance ratio is to use a large displacement between the beam and signal line. However, if the height of the beam was changed too high, the reliability of MEMS switches would be degraded, then, the actuation voltage would be altered.

At present, there also have been several attempts (Angira et al. 2013; Park and Kim 2000; Park et al. 2001; Persano et al. 2010) to use high dielectric constants materials include $HfO_2(\varepsilon_r = 20)$, STO($\varepsilon_r$ = 30–120), Ta_2O_5 ($\varepsilon_r = 32$) to obtain a high on/off capacitance ratio. As a result, the capacitance ratio of switches are more than 100. Meanwhile, some approaches of designing low spring

✉ Kun Deng
dengkun@bupt.edu.cn

Fuxing Yang
yangfx@bupt.edu.cn

Zhongliang Deng
dengzhl@bupt.edu.cn

Xuanming Wang
siegfeerd@sina.com

Ke Han
hanke@bupt.edu.cn

[1] School of Automation, Beijing University of Posts and Telecommunications, Haidian District, Beijing 100876, China

[2] School of Electronic Engineering, Beijing University of Posts and Telecommunications, Haidian District, Beijing 100876, China

constants to get a low actuation voltage just under 10 V have been proposed, for example, Ya et al. (2013) design on COMS RF MEMS switch managed to achieve a low actuation voltage of 3 V, but the relatively wide beams cannot be easily released with membrane in one step. Yongqing et al. (2018) achieved a switch with 14 V actuation voltage, which can be mounted on frequency reconfigurable antenna. Gopalan and Kommuri (2018) achivevd a triangular series RF MEMS switch with 5.6 V actuation voltage and as low as 5 MPa stress, which can be potentially used to build the miniature phase shifter. Ma et al. (2016) design on a low actuation voltage switch of 3 V, however, the beam of 1.397 μm thickness is very thin, which will cause the instanbility. Rousstia et al. (2015) designed a RF MEMS switch, which can be combined with the array antenna and achieve a good directivity and gain of the antenna.

This letter reports a novel RF MEMS switch with a $Si_3N_4(\varepsilon_r = 7.6)$ dielectric lyaer and a relactively lower air gap (2 μm), as shown in the Fig. 1. The MEMS switche have a Metal–insulator-metal (MIM) fixed capacitors, which can improve the capactances ratio without degrading the reliability of the switches. In order to obtain a low actuation voltage, the switch is designed in the form of bilateral drop-down electrodes and has a special beam like mechanical spring with a thickness of 1.6 μm, which can greatly reduce the spring constant. According to simulation analysis and parameter fitting, the capacitance ratio and actuationvoltage of the switch are 162 and 4.5 V respectively.

2 Circuit topology and theory analysis

2.1 Design MIM fixed capacitor to improve capacitance ratios

The circuit topology of the typical MEMS switch is as shown in Fig. 2a (Yang et al. 2014), when the MEMS switch is in up-state, the CPW-insulator-air-beam (Metal-Isulator-Air-Metal) fixed capacitors and edge capacitance C_f together form the upstate capacitance C_u; and when the switch is in down-state, the capacitance C_d is CPW-insulator-beam (Metal–insulator–Metal) fixed capacitors. The capacitive ratio C_r of the MEMS switch can be calculated from formuls (1) and (2) (Yang et al. 2014):

$$C_r = \frac{C_u}{C_d} = \frac{\frac{\varepsilon_0 \varepsilon_r A}{t_d}}{\frac{\varepsilon_0 A}{g + \frac{t_d}{\varepsilon_r}} + C_f} \tag{1}$$

where $\varepsilon_0, \varepsilon_r, t_d, g, A$ are the vacuum dielectric constant, relative dielectric constant of the dielectric layer, the thickness of the dielectric layer, the gap between the beam and the electrodes the cross-sectional area of the electrode.

The formula (1) can be simplified as (2), when C_f is ignored:

$$C_r = \frac{C_u}{C_d} = \frac{\frac{\varepsilon_0 \varepsilon_r A}{t_d}}{\frac{\varepsilon_0 A}{g + \frac{t_d}{\varepsilon_r}}} = \frac{g \varepsilon_r}{t_d} + 1 \tag{2}$$

In this paper, a MIM capacitor is designed on the signal line to improve capacitance ratio, as shown in Fig. 2b. When in up-state, MIM capacitor connects to a MAM capacitor in series, and the MAM is changed to resistance R in down-state. Then, the C_r can be calculated as follows, C_f is ignored:

$$\begin{aligned} C_r = \frac{C_d}{C_r} = \frac{C_{MIM}}{C_{MIM} \parallel C_{MAM}} = \frac{C_{MIM}}{C_{MAM}} + 1 \\ = \frac{\varepsilon_r g}{t_d} \frac{A_{MIM}}{A_{MAM}} + 1 = \frac{\varepsilon_r g}{t_d} \lambda + 1 \end{aligned} \tag{3}$$

$$C_{MAM} = \frac{\varepsilon_0}{g} A_{MAM}, C_{MIM} = \frac{\varepsilon_0 \varepsilon_r}{t_d} A_{MIM} \tag{4}$$

where λ is equal to A_{MIM}/A_{MAM}, other parameters are defined as same as formulas before. As shown in Fig. 3, for traditional MEMS switches, with t_d is not less than 0.15um and g is more than 1um, the C_r is less than 150. Due to loading MIM fiexd capacitor, C_r is increased with the increase of the value g and λ, as shown in Fig. 3b.

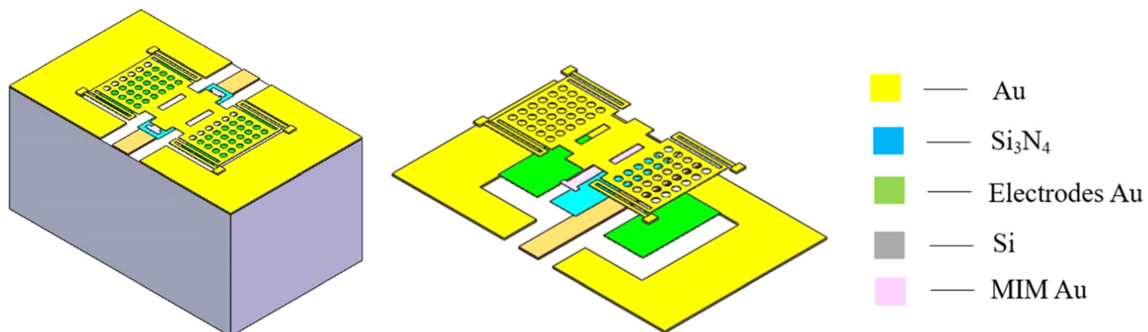

Fig. 1 Switch diagram

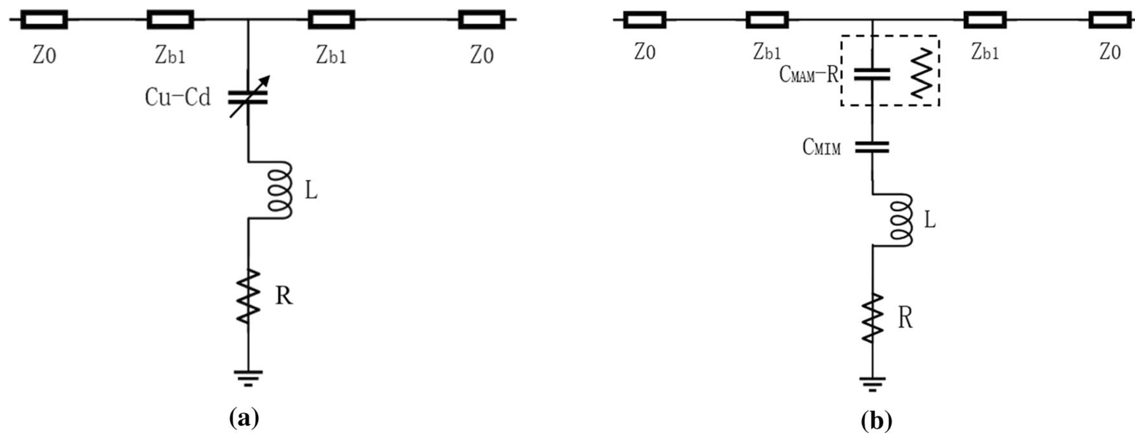

Fig. 2 Circuit topology of MEMS switches: **a** circuit models of traditional MEMS switches; **b** circuit model of the proposed MEMS switch with MIM capacitors

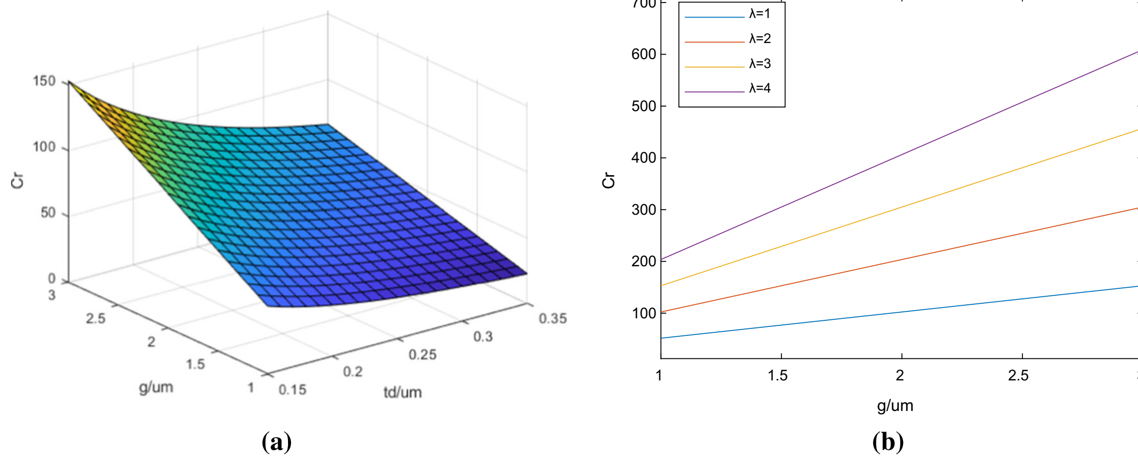

Fig. 3 The relationship among g, t_d, λ and C_r. **a** The value of C_r, when $g > 1$ μm, $t_d > 0.15$ μm. **b** The relationship among λ g and C_r

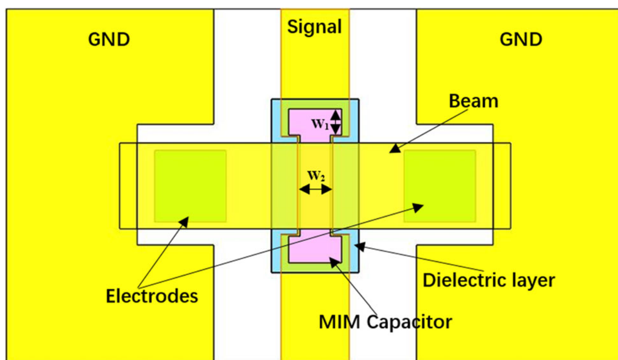

Fig. 4 The schematic view of the MEMS switch

As shown in Fig. 4, the MEMS switch loads a MIM capacitor on the signal line, in order to ensure a beam contacts the MIM capacitor when the switch is in down-state, RF and DC electrodes are separated designed.

For the switch based on high-resistance silicon ($\varepsilon_r = 11.9$), the CPW line is 60/100/60(G/S/G) μm, and the size of the beam is w_beam = 220 μm, l_beam = 500 μm. Si_3N_4 is used as dielectric material, and the thickness of Si_3N_4 is 0.15 μm. The capacitance Cu of the switch without MIM capacitors can be calculated simply as 57.8fF (Yang et al. 2014), and $C_r \approx 55$. For the switch with MIM capacitors, Fig. 5 shows the relationship among the parameter of $w1$, $w2$, and C_r.

It can be found the value of C_r has been significantly improved with MIM capacitors. When $w_1 = 10$ μm, Cr is increased with the increase of the value of w_2. And when $w_2 = 30$ μm, C_r is descreased with the increase of the value of w_1. It can be found $C_r = 206$ with $g = 2$ μm, $t_d = 0.15$ μm, $w_1 = 10$ μm, $w_2 = 30$ μm.

2.2 Electrodes topology and spring constant analysis

As shown in Fig. 6, in order to reduce dielectric charging effects and increase switches service life, the electrodes sit

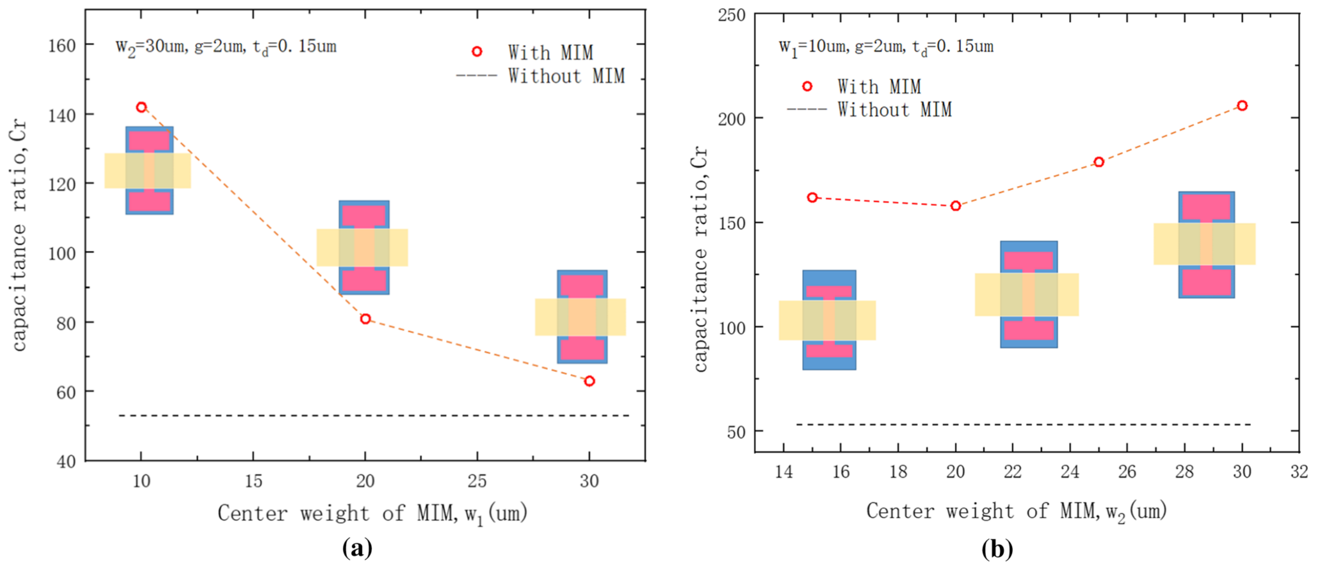

Fig. 5 Comparison of C_r with and without MIM. **a** The relationship among the value of C_r and w_1. **b** The relationship among the value of C_r and w_2

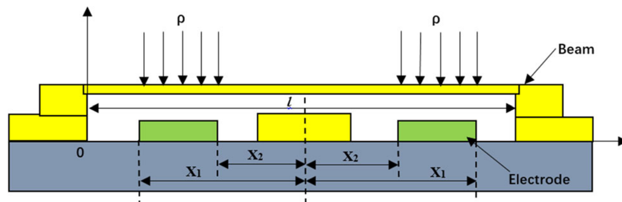

Fig. 6 Electrodes topology of the MEMS switch

on opposite sides of the center signal line. x_1 and x_2 represent the coordinate positions of the electrodes. In this form of electrodes, the spring constant k of MEMS switches can be calculate as follows (Deng et al. 2016)

$$k_1 = -\frac{P}{\frac{2}{EI}\int_{l/2+x_2}^{l/2+x_1} \frac{\rho}{48}(l^3 - 6l^2a + 9la^2 - 4a^3)da} = -\frac{48EI(x_1 - x_2)}{-\frac{1}{4}l^3x_1 + \frac{1}{4}l^3x_2 + lx_1^3 - lx_2^3 - x_1^4 + x_2^4} \tag{5}$$

$$k_2 = \frac{P}{2\int_{l/2+x_2}^{l/2+x_1} \frac{\rho}{2S}(l - \mathrm{a})da} = -\frac{4S}{x_1 - x_2 + l} \tag{6}$$

$$k = k_1 + k_2 \tag{7}$$

$$I = \frac{wt^3}{12} \tag{8}$$

$$P = 2\rho(x_1 - x_2) \tag{9}$$

$$S = \sigma(1 - v)tw \tag{10}$$

where k_1 is the spring constant caused by stiffness of the beam, k_2 is the spring constant caused by biaxial residual stress of the beam, ρ is uniformly distributed load of the beam, S is the tensile force of biaxial residual stress, σ is biaxial residual stress, v is the Possion ratio, E is the Young's modulus, and w is the width of the beam.

The actuation voltage of the MEMS switch can be given by (11):

$$V_p = \sqrt{\frac{8k}{27\varepsilon_0(2w(x_1 - x_2))}g^3} \tag{11}$$

The relationship between the spring constant and the coordinates of the electrodes is shown in Fig. 7. It can be seen the spring constant is increased with the increase of

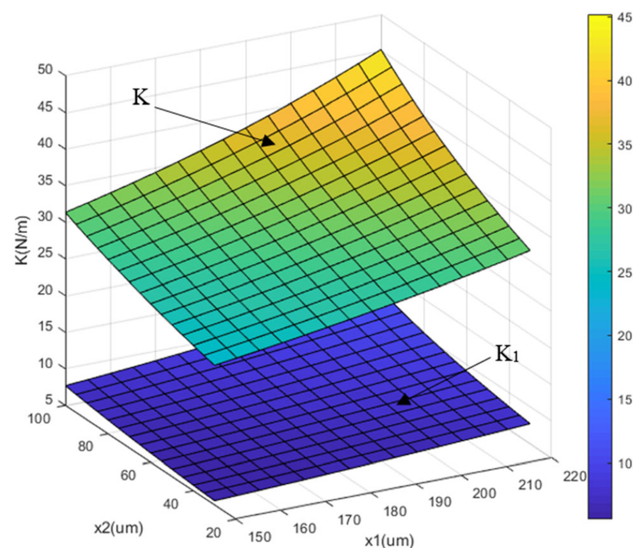

Fig. 7 The relationship between the x_1, x_2 and k_1, k

the area of electrodes. For the rectangle beam with Au (E = 78Gpa, v = 0.44), the length is 500 μm, the weight is 220 μmm, the gap is 2 μm and σ = 10 Mpa, it can be found when x_1 = 180 μm and x_2 = 70 μm, k_1 = 7.6 N/m, k = 31.34 N/m, the spring constant caused by biaxial residual stress is dominant.

As shown in Fig. 8, the actuation voltage V_p is changed with the change of values of (x_1, x_2), and a minimum value of V_p can be obtained in the range of values of (x_1, x_2). When the values of (x_1, x_2) are in regions 1 and 2, $V_p \leq 10$ V.

As shown in Fig. 9, the actuation voltage V_p and the spring constant caused by biaxial residual stress is increased as σ increases. For the rectangle beam with Au (E = 78 Gpa, v = 0.44), the length is 500 μm, the weight is 220 μmm, the gap is 2 μm, x_1 = 180, x_2 = 70;when $V_{p} \leq 20$ v, $\sigma \leq 30$ Mpa.

3 Design and simulation

3.1 Low spring constant switch design and analytical pull-in model

This paper designs the switch structure as shown in Fig. 10a. The beam adopts a structure similar to mechanial spring, which is fixed on the ground by four anchor points. Cantilever beams are normally insensitive to the biaxial residual stress but are very sensitive to the stress gradient due to their free-end condition. Slotting the beam can not only reduce the spring constant but also increase the inductance of the switch.

For simplicity, we adjusted 'paralle-plate approximation' to the moveble plate, as seen in Fig. 10b, and spring-mass model can be used to determine the relationships between the pull-in voltage and the dimensional parameters of the switch (Yang et al. 2014). The spring constants of the membrane can be described as follows.

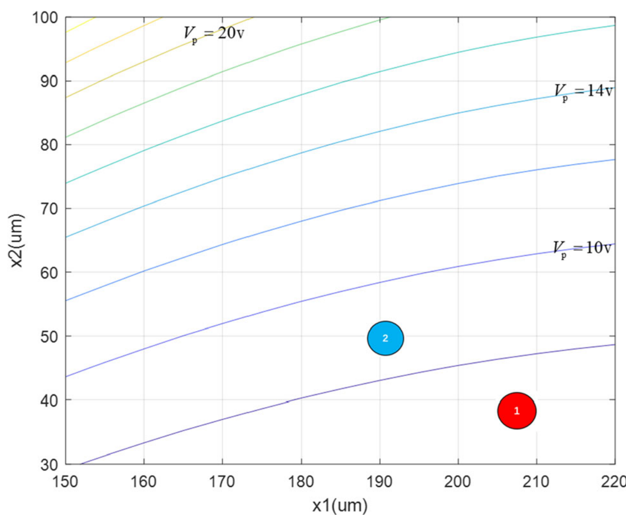

Fig. 8 The relationship between the x_1, x_2 and V_p

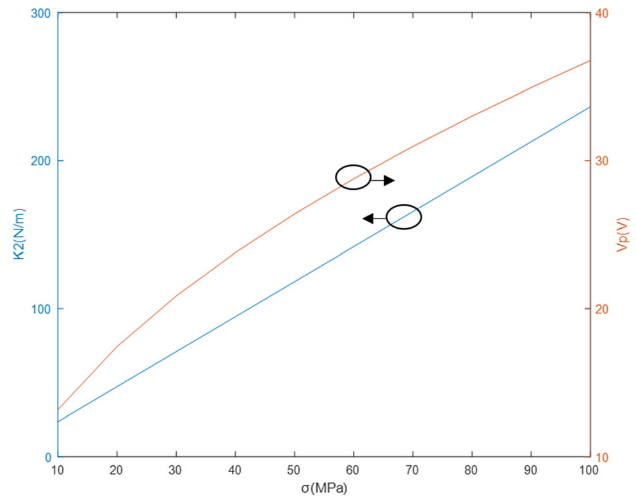

Fig. 9 The relationship between the σ and the k_2 and V_p

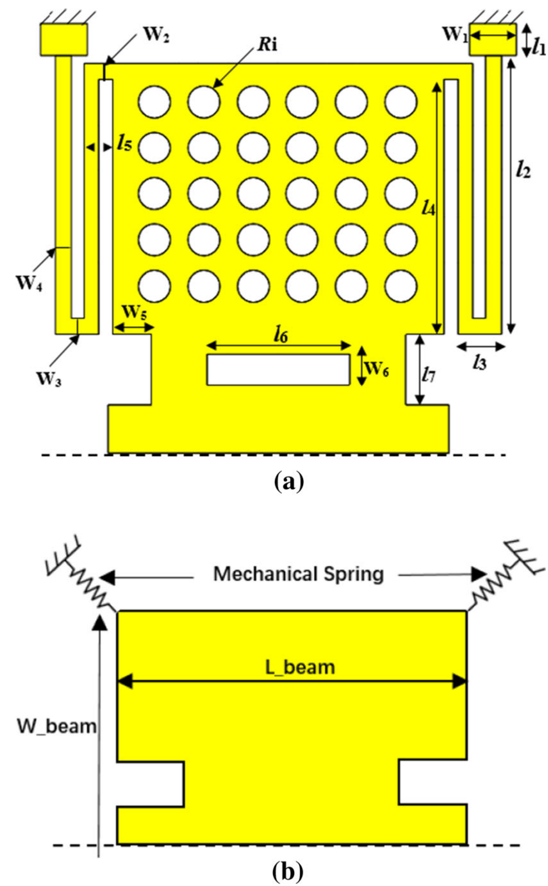

Fig. 10 a Detailed dimensions of membrane part in the switch, b switch with simple mechanical spring

$$k_1 = 4Ew_1\left(\frac{t_a}{l_1}\right)^3, \quad k_2 = 4Ew_2\left(\frac{t}{l_5}\right)^3 \tag{12}$$

$$k_4 = 4Ew_4\left(\frac{t}{l_2 + l_4}\right)^3, \quad k_3 = 4Ew_3\left(\frac{t}{l_3}\right)^3 \tag{13}$$

where w_1, w_2, w_3, w_4, l_1, l_2, l_3, l_4 are labeled in Fig. 10a. E is the Young's modulus of the structural material, t_a is the thickness of the anchor point, t is the thickness of the beam. Ignore the spring constant caused by biaxial residual stress of the beam, the total spring constant of the switch can be calculated as

$$k_{total} = (k_1 \parallel k_2 \parallel k_3 \parallel k_4) \tag{14}$$

In addition, the overlap area between the beam and two bottom electrodes can be calculated as

$$A_{total} = 2(S_e - N\pi(Ri)^2) \tag{15}$$

where R_i is also shown in Fig. 10a, S_e is the area of elelctrode, N is the number of slots above the electrode. From (12) and (15), the actuation voltage of the switch can be calculated as

$$V_p = \sqrt{\frac{8k_{total}(g + t_d/\varepsilon_r)^3}{27\varepsilon_0 A_{total}}} \tag{16}$$

where ε_r and ε_0 are the relative permititivity of the dielectric layer and the permittivity of an air, respectively.

For the switch beam with Au (E = 78Gpa, v = 0.44), the length is 500 μm, the weight is 220 μmm, the gap is 2 μm, Other physical dimensions of beams are shown in Table 2. As shown in Fig. 11, with the help of finite element analysis software, deformation of the beam under different thickness are analyzed, and all three models are under same loading form of both sides. When the thickness of beam are 1 μm, 1.6 μm and 2 μm, respectively, the spring constance are 0.7392 (N/m), 1.6215 (N/m) and 4.3571 (N/m), and the corresponding voltage can be calculated to 2 V, 4.5 V and 9 V.

The maximum stress occurs in the position shown in the Fig. 12, which is the most likely point of failure in the working state. The max stress is 8 Mpa with the thickness of beam 1 μm, and it increases to 13 Mpa when the thickness of beam is 1.6 μm. The equivalent stress is smaller with t_beam = 1 μm, however, the thickness is too thin and flexed easily, which cannot fully contact with the dielectric layer, and this will results the signal that barrier effect is particularly poor. Therefore, beams of too small thickness cannot be selected.

Furthermore, Table 1 shows some other calculation parameters of the switch. It can be seen that the pull-down time and pull-up (Rebeiz 2004) time are decreasing with the increase of beam thickness, what's more the beams

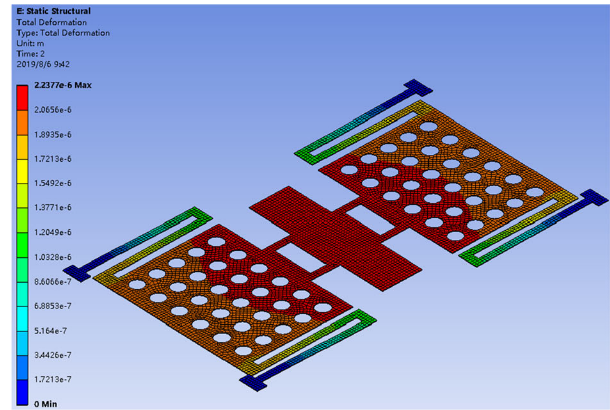

(a)

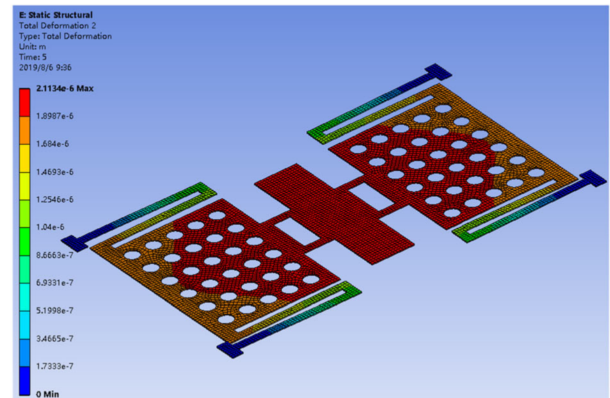

(b)

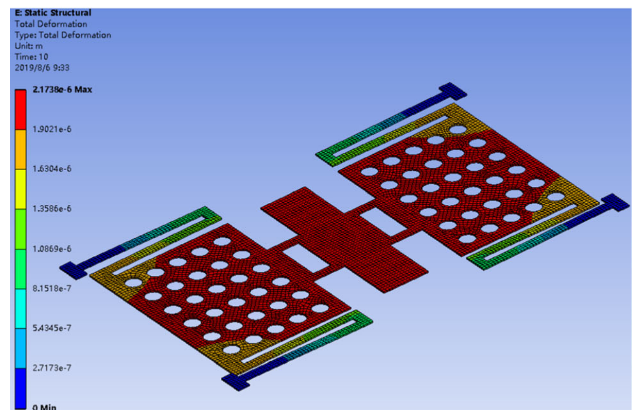

(c)

Fig. 11 Deformation diagram; **a** both sides loading and t_beam = 1 μm, **b** both sides loading and t_beam = 1.6 μm, **c** both sides loading and t_beam = 2 μm

with thin thickness are less stable. And compared to 2 μm, 1.6 μm thick beam is more economical in the process of material saving.

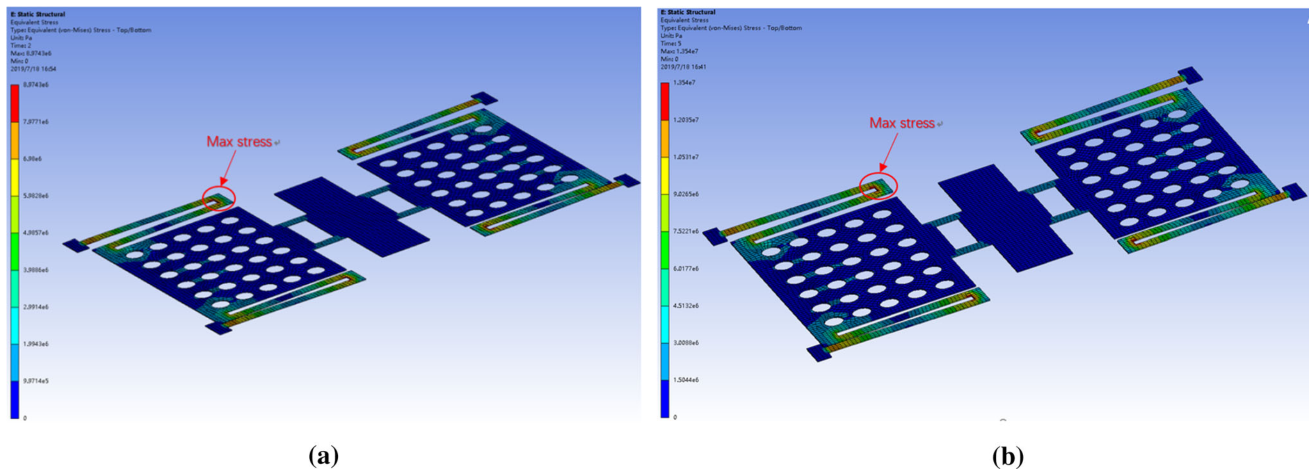

(a) (b)

Fig. 12 Equivalent stress diagram; **a** both sides loading and *t*_beam = 1 μm, **b** both sides loading and *t*_beam = 1.6 μm

Table 1 Switch parameter

Beam thickness (μm)	Actuation voltage (V)	Max stress (MPa)	Resonant frequency (Hz)	Pull-down time (us)	Pull-up time (us)
1	2	8	2207	189	113
1.6	4.5	13	3521	118	71
2	9	22	4391	95	57

3.2 Physical demensions of the proposed switch

Through the above analysis, physical demensions of the proprosed switch are shown in Table 2. In this paper, we use Au as the beam material, Si_3N_4 as the dielectric material, and high resistivity silicon substrate.

3.3 Simulation of S-parameters

As shown in Fig. 13(a), the thickness of beam t_beam has a influence on resonant frequency. When the size of t_beam is increased, the resonant frequency increases gradually. Under the condition of different thickness, the isolation is less than − 20 dB within the range of 10–30 GHz, and the extreme value reaches − 45 dB. As shown in Fig. 13b, the return loss is less than − 12 dB at the resonant frequency.

Figure 14 shows the relationship between the value of w_7, w_8 and isolation, when the size of the upper metal layer of the MIM capacitor is increased, the resonant frequency of MEMS switch is decreased due to the increase of the shun capacitance. When the size of MIM capacitor is $w_7 = 30$ um, $w_8 = 10$ um, the resonant frequency of MEMS switch is 21.5 GHz, and the isolation reaches − 40 dB.

We can see from Fig. 15a, when the switch is in up-state, the current can be transmitted better on the signal line, and its main energy is concentrated on both sides of the transmission line. A small amount of energy is coupled

Table 2 Physical demensions of the switch

Symbols	Descriptions	Values
l_1	Length of the anthor	15 μm
l_2	Length in the mechanical spring	170 μm
l_3	Length in the mechanical spring	30 μm
l_4	Length in the rectangular plate	150 μm
l_5	Length in the mechanical spring	20 μm
l_6	Length of the rectangular hole	60 μm
l_7	Length in the rectangular plate	50 μm
l_{beam}	Length of the beam	500 μm
w_1	Weight of the anthor	30 μm
w_2	Weight in the mechanical spring	20 μm
w_3	Weight in the mechanical spring	10 μm
w_4	Weight in the mechanical spring	10 μm
w_5	Weight in the rectangular plate	70 μm
w_6	Weight of the rectangular hole	30 μm
w_7	Weight in the MIM capacitor	30 μm
w_8	Weight in the MIM capacitor	10 μm
w_{beam}	Weight of the beam	220 μm
N	Number of round holes	56
R_i	Radius of the hole	4 μm
t_{beam}	Thickness of the beam	1.6 μm
t_d	Thickness of the dielectric layer	0.15 μm
t_{MIM}	Thickness of the MIM capacitor	1 μm
S_e	Area of the electrodes	100*150 μm^2
G	Air gap	2 μm
ε_r	Relative permitticity of dielectric layer	7.6

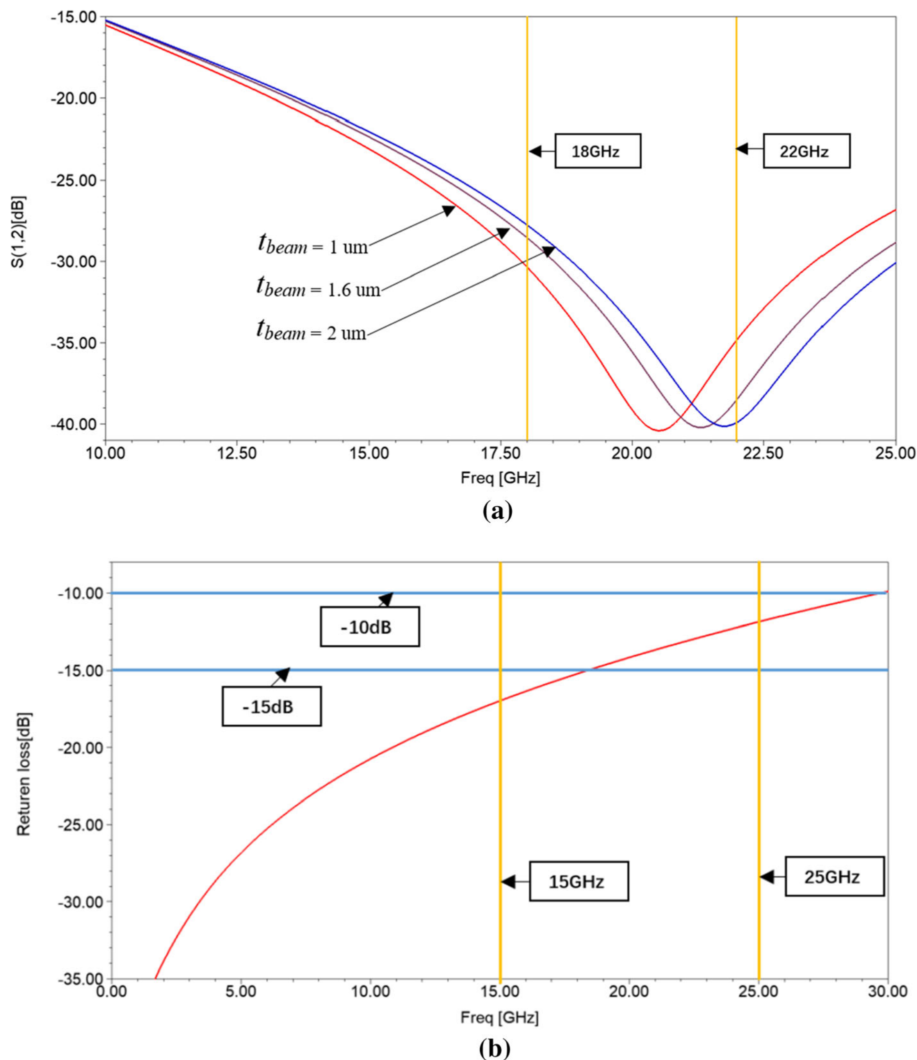

Fig. 13 S12 and S11 for the switch. **a** Isolation for different thickness beam of the switch. **b** Returen loss for the switche with 1.6 μm thickness beam

with the beam, and consumption is very small. When the switch is in down-state, Fig. 10b, the signal is blocked by the beam and cannot be transmitted to the other side, most energy is reflected back. Therefore, the current value on the side of the transmission line is higher than it in up-state. Some energy is transmitted through the beam to the ground.

3.4 Analysis

In this paper, the beam structure like mechanical spring can be drastically reduced the value of spring constance due to cantilever beams are normally insensitive to the biaxial residual stress but are very sensitive to the stress gradient. Meanwhile, when the thickness of the beam is decreased, the actuation voltage decrease, however, the thickness is too thin and flexed easily, which cannot fully contact with the dielectric layer, the signal that barrier effect is particularly poor. In this paper, the thickness of the beam is 1.6 μm.

For the MEMS switches, Cu, Cd, L and R can be extracted from the return loss S11 and isolation S12. The RF MEMS switch and CPW transmission line consist of three parts and can be expressed by ABCD matrix (Pozar 2009):

$$\begin{pmatrix} A & B \\ C & D \end{pmatrix} = \mathrm{M_1 M_2 M_1} \tag{17}$$

where $\mathrm{M_1}$ represents the CPW transmission line part (the ABVD matrix consist of two M1 for the symmetry). $\mathrm{M_2}$ represents the lumped parameter model of the RF MEMS. They are:

$$\mathrm{M_1} = \begin{pmatrix} \cos\theta & jZ_0 \sin\theta \\ j\dfrac{1}{Z_0}\sin\theta & \cos\theta \end{pmatrix} \tag{18}$$

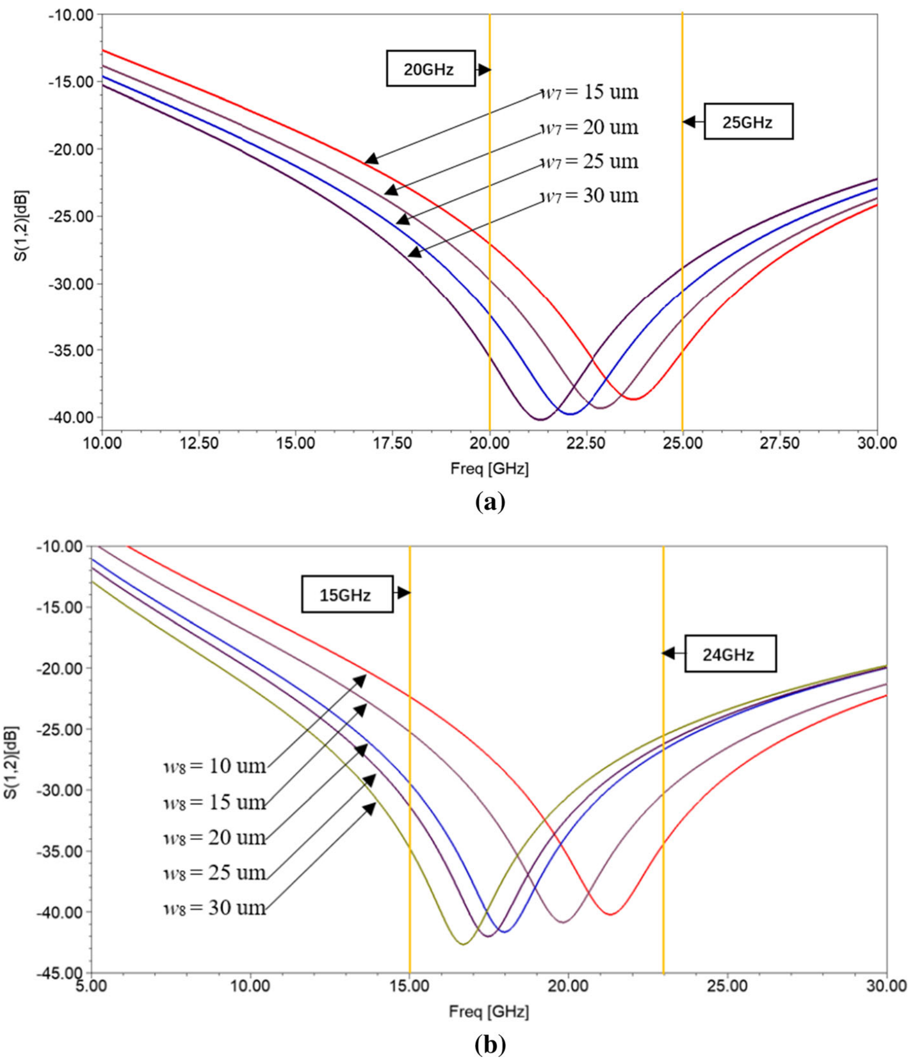

Fig. 14 S12 for the switch with different MIM capacitors; **a** different weight in the MIM capacitor w7, **b** different weight in the MIM capacitor w8

$$M_2 = \begin{pmatrix} 1 & 0 \\ Y_2 & 1 \end{pmatrix} \tag{19}$$

where θ is CPW transmission line electric length, Z_0 is the characteristic impedance of transmission line, Y_2 is:

$$Y_2 = \frac{1}{(jwC_s)^{-1} + jwL + R_s} \tag{20}$$

where C_s is C_{up} or C_{dw} when the switch stays the corresponding state. The expression $L = (wC_s) - 1$ is satisfied when the switch operates at the resonant frequency. R_s is the loss resistance. S21 is:

$$S_{21} = \frac{2}{A + B/Z_0 + CZ_0 + D} \tag{21}$$

From Eqs. (17)–(22), for the proposed switch, C_u = 26.5 fF, C_d = 4.3 pF, C_r = 162, the MIM capacitors can improve the on/off capacitance ratio without adding more less to the switches.

Table 3 shows the comparison of this paper with other developed capacitive RF-MEMS switch. It presents that the proposed switch have a lower actuation voltage with excellent electromagnetic characteristics than others.

4 Conclusions

In this paper, a novel type high on/off capacitance ratio and low actuation voltage RF MEMS switch has been designed. The switch is in the form of bilateral drop-down electrodes and has a special beam like mechanical spring with a thickness of 1.6 µm, which can greatly reduce the spring constance. The actuation voltage is as low as 4.5 V by finite element analysis software simulation. MIM capacitors can improve the on/off capacitance radio and can also ensure good electrical isolation performance. From the fitted results, the on/off capacitance ratio is 162 for the MEMS switch. Through the use of HFSS software analysis,

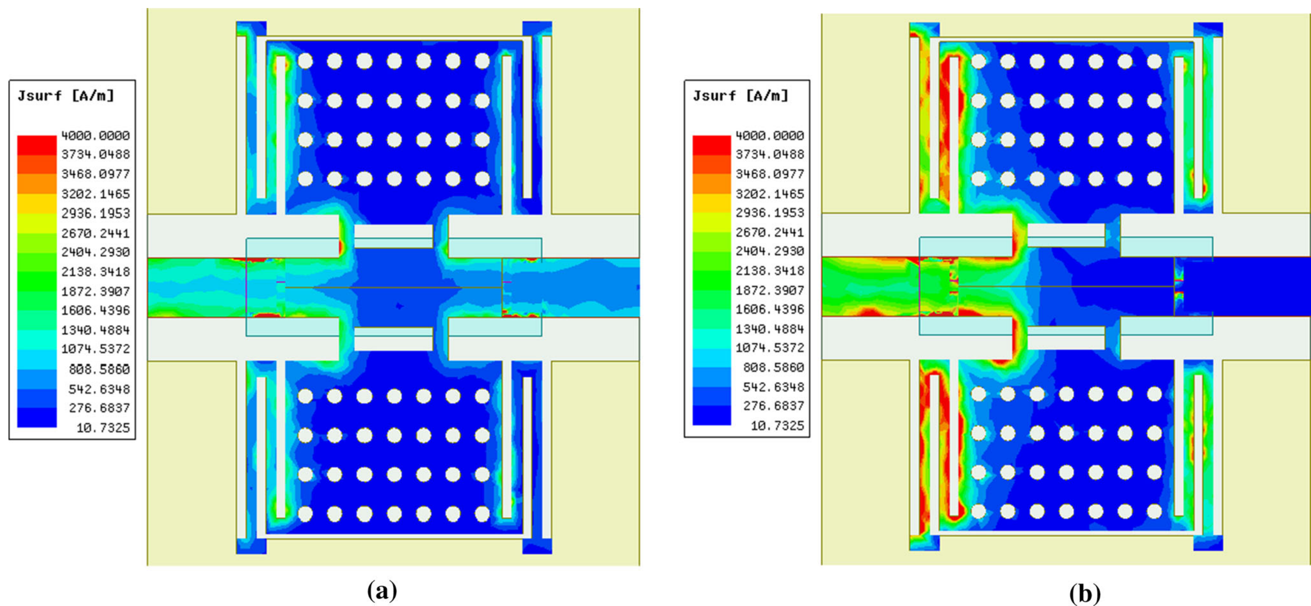

Fig. 15 Current diagram; **a** switch in up-state, **b** switch in down-state

Table 3 Comparison of developed capacitive RF-MEMS switches

Years	Authors	C_{up} (fF)	C_{down} (pF)	C_r	Insertion loss (dB) (GHz)	Isolation (dB) (GHz)	Actuation voltage (V)
2011	Persano A	70	1.32	18.8	< 0.8@30	38@23	15–20
2012	Badia MF-B	–	1.27	–	0.68@40	35.8@40	23.6
2013	Fall M	4.8	0.16	33.3	0.3@20	< 1.5@20	38
2014	Deepak B	–	–	–	< 0.1@20	43@9.5	20
2016	Li-Ya Ma	140	7.31	52	5.65@40	24.38@40	3.04
2018	Xu YQ	–	–	–	0.1@30	26@30	14
2018	Ke Han	54	20.8	385	< 0.5@40	34@10	21
This paper	–	26.5	4.3	162	< 0.2@30	41@22	4.5

within the range of 10–30 GHz, the up-state insertion loss is better than − 0.2 dB, the down-state isolation is better than − 20 dB, and the minimum isolation is − 41 dB at resonant frequency.

Acknowledgements The authors sincerely thanks to Wireless Network Location and Communication Fusion Laboratory, Beijing University of Posts and Telecommunications for their support. This work was supported by the joint fund of ministry of education for equipment pre-research (2017), Grant Number 6141A02022403.

References

Angira M et al (2013) On the investigation of an interdigitated, high capcacitance ratio shunt RF-MEMS switch for X-band applications. Proc NSTI Nanotechnol 2:189–192

Badia MF-B, Buitrago E, Ionescu AM (2012) RF MEMS shunt capacitive switches using AlN compared to Si_3N_4 dielectric. J Microelectromech Syst 21(5):1129–1240. https://doi.org/10.1109/jmems.2012.2203101

Bansal D, Kumar A, Sharma A et al (2014) Design of novel compact anti-stiction and low insertion loss RF MEMS switch. Microsyst Technol 20:337–340. https://doi.org/10.1007//s00542-013-1812-1

Cook EH, Tomaino-Iannucci MJ, Reilly DP et al (2018) Low-power resonant acceleration switch for unattended sensor wake-up. J Microelectromech Syst 27(6):1071–1074. https://doi.org/10.1109/jmems.2018.2867282

Deng Z, Wei H, Fan S, Gan J (2016) Design and analysis a novel RF MEMS switched capacitor for low pull-in voltage application. Microsysy Technol 22:2141–2149

Fall M, Fouladi S, Domingue F et al (2013) High capacitance ratio RF MEMS dielectric-less switched capacitor. Microwave Integrated Circuits Conference (EuMIC), 2013 European. IEEE

Gopalan A, Kommuri UK (2018) Design and development of miniaturized low voltage triangular RF MEMS switch for phased array application. Appl Surf Sci 2018(449):340–345. https://doi.org/10.1016/j.apsusc.2018.02.210

Han K, Guo X, Smith S, Deng Z, Li W (2018) Novel high-capacitance-ratio MEMS switch: design analysis and performance verification. Micromachines 9:390. https://doi.org/10.3390/mi9080390

Ma L-Y, Nordin AN, Soin N (2016) Design, optimization and simulation of a low-voltage shunt capacitive RF-MEMS switch. Microsyst Technol 2016(22):537–549. https://doi.org/10.1007/s00542-015-2585-5

Metta K, Bansal D, Bajpai A, Kumar P (2018) Improved isolation RF MEMS switch with post release ashing. Microsyst Technolo 24:3863–3886. https://doi.org/10.1007/s00542-018-3865-7

Michalas L, Koutsoureli M, Papandreou E, Giacomozzi F (2015) Dielectric charging effects in floating electrode MEMS capacitive switches. Microelectron Reliab. 55(10):1891–1895. https://doi.org/10.1016/j.microrel.2015.07.024

Park JY, Kim GH, Chung KW et al (2000) Fully intergrated micromachined capacitve switches for RF applications. Microwave Symposium Digest IEEE Mtt-s International. IEEE

Park JY, Kim GH, Chung KW et al (2001) Monolithically integrated micromachined RF MEMS capcacitive switches. Sens Actuators A Phys 89(1–2):88–94

Persano A, Fabio Q , Adriano C et al (2010) Ta^2O^5 thin films for capacitive RF-MEMS switched. J Sens 2010(1687-725X):23–59

Persano A, Cola A, Angelis GD et al (2011) Capacitive RF MEMS switches with tantalum-based materials. J Microelectromech Syst 20(2):365–370. https://doi.org/10.1109/jmems.2011.2107884

Pozar DM (2009) Microwave engineering. Wiley, New York

Rebeiz GM (2004) RF MEMS: theory, design, and technology. Wiley, New York

Rousstia MW, Reniers ACF, Herben MHAJ (2015) Switched-beam array of dielectric rod antenna with RF MEMS switch for millimeter-wave applications. Radio Sci 50(3):177–190. https://doi.org/10.1002/2014RS005471

Ya ML, Nordin AN, Soin N (2013) Design and analysis of a low voltage electrostatic actuated RF CMOS-MEMS switch. Micro and Nanoelectronics (RSM), 2013 IEEE Regional Symposium on. IEEE

Yang HH, Zareie H, Rebeiz GM (2014) A high power stress-gradient resilent RF MEMS capative switch. J Microelectromech Syst 24(3):599–607

Yongqing Xu, Tian Y, Zhang B, Duan J, Yan Li (2018) A novel RF MEMS switch on frequency reconfigurable antenna application. Microsyst Technol 24:3833–3841. https://doi.org/10.1007/s00542-018-3863-9

Publisher's Note Springer Nature remains neutral with regard to jurisdictional claims in published maps and institutional affiliations.